Research Square

Preprints are preliminary reports that have not undergone peer review.
They should not be considered conclusive, used to inform clinical practice,
or referenced by the media as validated information.

Genomic and metabolic insights into putative mannitol metabolism and marine adaptation of a Bacillus velezensis isolate from barnacle biofilm

Naufal Baariq
University of Indonesia
Masafumi Yohda
Tokyo University of Agriculture and Technology
Hanna Aulia Mumtaz
University of Indonesia
Ibnu Maulana Hidayatullah
University of Indonesia
Atsushi Arakaki
Tokyo University of Agriculture and Technology
Heri Hermansyah
University of Indonesia
Muhamad Sahlan
sahlan@che.ui.ac.id

University of Indonesia

Research Article

Keywords: Bacillus velezensis, barnacle biofilm, mannitol metabolism, pan-genome, whole-genome sequencing, HAD phosphatase

Posted Date: November 23rd, 2026

DOI: https://doi.org/10.21203/rs.3.rs-11442792/v1

License: This work is licensed under a Creative Commons Attribution 4.0 International License.
Read Full License

Additional Declarations: No competing interests reported.

Abstract

Barnacle biofilms host bacteria whose metabolism may be relevant to marine biotechnology, but few isolates from this habitat have been characterized at the genome level. Here we sequenced and analyzed the genome of a *Bacillus velezensis* isolate from barnacle biofilm, with emphasis on mannitol metabolism. The assembly comprised 49 contigs (3,891,584 bp; GC content 46.35%), and average nucleotide identity and digital DNA–DNA hybridization placed the isolate within *B. velezensis*. A pan-genome analysis with four reference genomes yielded 4,303 gene clusters, of which 3,375 formed the core genome, and the 76 isolate-specific clusters were dominated by mobile genetic elements. The genome encoded the mannitol phosphotransferase system and mannitol-1-phosphate dehydrogenase but no annotated mannitol-1-phosphatase, and six haloacid dehalogenase (HAD) superfamily phosphatases were nominated as candidates for the missing step. Mannitol was nevertheless detected by high-performance liquid chromatography in culture supernatants, at 44.70 ± 1.25 mg/L with glucose and 63.96 ± 1.11 mg/L with fructose, which suggests that the candidate phosphatases may have the potential to complete the route, although it does not identify the responsible enzyme. The isolate also carried conserved osmoadaptive and biofilm-related systems, 18 biosynthetic gene clusters, cell wall hydrolases and fermentative pathways. These results define the mannitol route of the isolate as putative and identify the phosphatase step as the target for biochemical validation.

1. Introduction

Mannitol is a carbohydrate compound belonging to the group of sugar alcohols, or polyols. Chemically, it is a six-carbon sugar alcohol ($C_6H_{14}O_6$) containing six hydroxyl (-OH) groups and is an isomer of sorbitol. Mannitol has a sweet taste, provides a cooling effect, and remains stable at high temperatures (Grembecka, 2015). These characteristics make it widely used as an alternative sweetener and an additive in various food products (Chen et al., 2020). Beyond the food industry, mannitol is also utilized in the pharmaceutical, chemical, and medical sectors for instance, in the production of nutritional tablets (Dai et al., 2017; Grembecka, 2015).

In nature, mannitol is commonly found in plants and microorganisms, such as algae, fungi, and bacteria (Dai et al., 2017; Jacobsen & Frigaard, 2014), where it serves functions including energy storage, the absorption of reducing power, the scavenging of reactive oxygen species, osmoregulation, and defense against pathogens (Iwamoto & Shiraiwa, 2005). Mannitol can be produced through extraction, chemical synthesis, or microbial fermentation (Dai et al., 2017).

Marine bacteria represent one group of microorganisms capable of metabolizing mannitol through interactions with various organic matter sources in the marine environment. Research by Groisillier et al., (2015) identified a number of genes present in the marine bacterium Zobellia galactanivorans. The presence of genes related to mannitol metabolism warrants further investigation, as a bacterium's ability to utilize this compound is not determined by a single gene alone; rather, it may involve multiple genes that play roles in transport, osmoregulation, and enzymatic reactions (Byer et al., 2017; Iwamoto &

Shiraiwa, 2005; Nguyen et al., 2019). Furthermore, the genetic organization of mannitol metabolic systems varies across different bacterial groups(Joshi & Xu, 2007). Consequently, gene identification must account for sequence homology, functional annotation, and the relationship between specific genes and known metabolic pathways (Fu et al., 2023). One effective approach is genomic sequence analysis via Whole Genome Sequencing (WGS), a comprehensive method for identifying genes that encode specific enzymes (Singh et al., 2024).

This research approach serves as the foundation for the current study, which utilizes bacteria isolated from barnacles to identify genes involved in mannitol metabolism. Barnacles are marine crustaceans belonging to the subclass Cirripedia, they are sessile organisms that attach themselves to hard surfaces, such as rocks, the shells of other organisms, ship hulls, and various marine structures (Ip et al., 2021). Excessive barnacle growth can lead to marine biofouling the accumulation of organisms that increases drag on vessels and raises maintenance costs(Hopkins et al., 2021; Petersen et al., 2020). Barnacles also host bacterial communities on their shell surfaces. While not all of these bacteria are harmful, many are associated with the marine environment (Bacchetti De Gregoris et al., 2012). One such group found in barnacles is the genus Bacillus, supported by research from Wismayanti et al., (2019)who successfully identified the activity of Bacillus cereus in barnacles. This reinforces a research approach aimed at identifying genes responsible for mannitol metabolism in the bacterium Bacillus velezensis found in barnacles. Bacillus velezensis is a capable bacteria of providing protection against osmotic stress by stabilizing cell structures and maintaining osmotic balance (Goszcz et al., 2026), which is a function served by mannitol in microorganisms.

2. Materials and methods

2.1. Sampling, isolation, and culture

Biofilm samples were collected from the surface of barnacles submerged approximately 1 m below the sea surface at Harapan Island, Kepulauan Seribu, Jakarta, Indonesia (5°44'40.6" S, 106°35'20.0" E). The samples were enriched in Marine Broth 2216 (HiMedia Laboratories, India; pH 7.0) and streaked onto MRS agar (HiMedia Laboratories, India; pH 5.6), both prepared according to the manufacturer's instructions. Individual colonies were purified by repeated streaking and cultivated in MRS broth at 30°C and 120 rpm for 42 h. One purified isolate was selected for whole-genome sequencing.

2.2. Genome annotation and functional characterization

Genomic DNA was extracted from the purified culture using the ZymoBIOMICS DNA Miniprep Kit (Zymo Research, Irvine, CA, USA) according to the manufacturer's instructions and sequenced on the Illumina MiSeq platform (paired-end reads). Reads were quality-filtered and adapter-trimmed with fastp v0.23.4 and assembled de novo with SPAdes v3.15.5 using default parameters. Assembly statistics (genome size, number of contigs, N50, L50, N90, L90, largest contig, and GC content) were calculated with QUAST v5.2.0, and completeness and contamination were estimated with CheckM2 v1.1.0.

2.3. Genome annotation and functional characterization

The assembly was annotated with Bakta v1.9.4 (database v5.0, full), which predicted protein-coding sequences, rRNAs, tRNAs, tmRNAs, ncRNAs, and pseudogenes. The translated protein set was functionally annotated with eggNOG-mapper v2.1.13 against the eggNOG database v5.0.2, with seed orthologs computed using DIAMOND, to assign COG categories, Gene Ontology terms, KEGG Orthology (KO) identifiers, EC numbers, KEGG pathways, and Pfam domains. Seed orthologs were assigned against *Bacillus velezensis* FZB42 (taxon 326423). Bakta and eggNOG-mapper were run on the Galaxy Europe platform (usegalaxy.eu). A circular genome map was generated with Proksee.

2.4. Taxonomic and phylogenomic identification

The genome was analyzed with the Type (Strain) Genome Server (TYGS; Meier-Kolthoff and Göker, 2019; results obtained on 20 September 2026). Because no 16S rRNA gene sequence was detected in the assembled genome, the automatic selection of closest type strains could not be completed, and ten type or reference strains were therefore selected manually. Pairwise genome comparisons were performed with the Genome BLAST Distance Phylogeny (GBDP) approach using the "trimming" algorithm and distance formula d5, with 100 distance replicates. Digital DNA–DNA hybridization (dDDH) values and confidence intervals were calculated with GGDC 4.0 using formula d4, and differences in G + C content were obtained from the same output. A balanced minimum evolution tree was inferred from the intergenomic distances with FastME 2.1.6.1 including SPR post-processing, with branch support from 100 pseudo-bootstrap replicates, and was rooted at the midpoint. Average nucleotide identity based on BLAST (ANIb) was calculated with JSpeciesWS (Richter et al., 2016) between the isolate (query) and the genomes of the type and reference strains. Species boundaries were interpreted using the commonly applied thresholds of 70% dDDH and 95–96% ANI.

2.5. Pan-genome analysis

Genomes of four *B. velezensis* references (NRRL B-41580, FZB42, KACC 13105, and KACC 18228) were retrieved from NCBI RefSeq and re-annotated with the same Bakta version as the isolate (v1.9.4, database v5.0), to minimize annotation-derived bias. Pan-genome analysis was performed with Panaroo v1.8.0 on the Bakta GFF3 files of the five genomes, in strict clean mode with the bacterial genetic code and otherwise default parameters, including a 98% sequence identity threshold for clustering, on the Galaxy Europe platform. Gene clusters present in all five genomes were defined as the core genome, those present in a subset of genomes as accessory, and those found only in the marine isolate as isolate specific. The gene presence–absence matrix was visualized as a heatmap using OriginPro 2026b (OriginLab Corporation, Northampton, MA, USA), and the intersections among genomes were visualized as an UpSet plot using the ComplexUpset package (Krassowski, 2020) in R v4.6.1.

2.6. Reconstruction of mannitol-related metabolic pathways

Genes of mannitol metabolism were identified in the Bakta and eggNOG-mapper annotations by gene name, EC number (2.7.1.197, 1.1.1.17, 3.1.3.22, 1.1.1.67, and 1.1.1.138), and KEGG Orthology (KO) identifier (K00009). KO assignments were mapped onto the fructose and mannose metabolism pathway (map00051) with KEGG Mapper (Search&Color; Kanehisa and Sato, 2020). The MtlD protein was compared with *B. velezensis* proteins by BLASTp against the database at NCBI, and its domains were taken from the Pfam annotations of eggNOG-mapper. Because no gene was assigned to mannitol-1-phosphatase, candidate sugar-phosphate phosphatases were selected from the haloacid dehalogenase (HAD)-superfamily proteins of the genome on the basis of their annotation, and their catalytic motif I (DxDx[T/V]) and Cof-type motif IV (GDxxND) were identified by pattern search of the protein sequences. Conserved domains of the candidates were examined with InterProScan 6 (Blum et al., 2026; InterPro release 110.0). The genomic neighborhood of the mannitol locus (11 genes, LOCUS_10350–LOCUS_10450, i.e., four genes upstream of mtlA and four genes downstream of mtlD) was extracted from the Bakta annotation and drawn with Python, and the conservation of each gene among the five genomes was taken from the Panaroo presence–absence table. Because the candidate phosphatases have not been tested experimentally, their functional assignments were treated as putative.

2.7. Fermentation and quantification of mannitol

A single colony of the isolate obtained on MRS agar (Section 2.1) was propagated in MRS broth at 30°C and 120 rpm until the optical density at 600 nm reached 0.8–1.0. This seed culture was inoculated at 10% (v/v) into MRS broth (pH 5.6) supplemented with 100 mg/L glucose or fructose, and fermentation was carried out at 30°C and 120 rpm for 42 h in [three independent flasks] per substrate, all inoculated from the same seed culture. Culture broth was centrifuged at 10,000 × g for 5–10 min until the supernatant was clear, and the supernatant was filtered through a 0.22 µm PTFE syringe filter before analysis. Mannitol was analyzed by HPLC on an Aminex HPX-87H column (Bio-Rad) at 50°C, with 0.005 N H_2SO_4 as the mobile phase at 0.5 mL/min and a refractive index detector at 50°C; the injection volume was 20 µL. Peaks were identified by comparison of retention times with authentic standards of mannitol, glucose, fructose and mannose, and mannitol was quantified with an external calibration curve (20–100 mg/L).

2.8. Comparative analysis of adaptive traits

Genes related to osmotic adjustment, ion homeostasis, general stress response, membrane fluidity, oxidative stress, and biofilm formation were identified in the Bakta and eggNOG-mapper annotations by gene name and KO identifier. Presence/absence and copy number of these systems were compared across the five genomes using the Panaroo gene presence–absence table. Genes of compatible-solute metabolism were additionally screened for the pathways of proline, glycine betaine, trehalose, and glutamate metabolism, and a pathway was considered not annotated when no gene with a matching name or KO was found.

2.9. Biosynthetic gene cluster prediction

Biosynthetic gene clusters (BGCs) were predicted with antiSMASH v6.1.1 (Blin et al., 2021) on the Galaxy Europe platform (run on 4 October 2026). The assembled genome (contig FASTA) was analyzed with the bacterial taxon setting, Prodigal gene finding, relaxed detection strictness, and a minimum contig length of 1,000 bp. KnownClusterBlast, SubClusterBlast, comparison against the MIBiG database bundled with antiSMASH 6.1.1, smCOG analysis, the active-site finder, and RREFinder were enabled. Similarity values are those reported by antiSMASH for the most similar known cluster. Regions located on a contig edge were flagged as possibly incomplete.

2.10. Cell wall–active enzymes and fermentative pathways

Carbohydrate-active enzymes (CAZymes) were annotated by submitting the 3,775 translated proteins (3,767 CDSs and 8 sORFs predicted by Bakta) to the dbCAN3 web server (Zheng et al., 2023; accessed [date]), which combines HMMER searches against the dbCAN HMM database, DIAMOND searches against the CAZy database, and dbCAN-sub searches. A protein was assigned to a CAZyme family only when it was supported by at least two of the three tools. Signal peptides were predicted with SignalP as implemented in dbCAN3. Cell wall–active proteins were selected from the Bakta and eggNOG-mapper annotations, and their domain organization was mapped with a custom Python script. Fermentation pathways were reconstructed manually from the Bakta and eggNOG-mapper annotations, and the pathway schematic was drawn with a custom Python script.

3. Results

3.1. Genome features and taxonomic placement

The draft genome of the isolate was assembled into 49 contigs with a total length of 3,891,584 bp and a GC content of 46.35% (Table 1). The largest contig measured 393,586 bp, and the N50 and L50 values were 120,401 bp and 11, respectively (N90 = 39,924 bp; L90 = 33). CheckM2 estimated a genome completeness of 100.0% with a contamination of 0.31%, indicating a high-quality draft assembly. Annotation predicted 3,767 CDSs with a coding density of 88.7%, together with 57 tRNAs, 1 rRNA, 1 tmRNA, 19 ncRNAs, and 7 pseudogenes.

Table 1
Genome features and assembly quality

Genomic feature	Value
Genome size (bp)	3,891,584
GC content (%)	46.35
Number of contigs	49
Largest contig (bp)	393,586
N50 (bp)	120,401
L50	11
N90 (bp)	39,924
L90	33
Genome completeness (%)	100.0
Contamination (%)	0.31
Coding density (%)	88.7
CDSs	3,767
tRNAs	57
rRNAs	1
tmRNAs	1
ncRNAs	19
Pseudogenes	7

Genome-based taxonomic analysis placed the isolate within the genus Bacillus, closest to *B. velezensis* (Table 2). Digital DNA–DNA hybridization (dDDH, formula d4) and average nucleotide identity (ANIb) values with the four *B. velezensis* reference genomes ranged from 84.2% to 91.1% and from 98.06% to 98.76%, respectively, the highest being with *B. velezensis* FZB42 (ANIb 98.76%; dDDH 91.1%). The type strain *B. velezensis* NRRL B-41580^T gave 98.06% ANIb and 84.2% dDDH. All these values exceed the commonly used species thresholds (≈ 95–96% ANI and 70% dDDH). The isolate showed lower relatedness to *B. siamensis* KCTC 13613^T (ANIb 93.97%; dDDH 56.8%) and *B. amyloliquefaciens* DSM 7^T (93.31%; 55.1%). Values to *B. nakamurai* NRRL B-41091^T (85.48%; 30.8%) and *B. tequilensis* NCTC 13306^T (76.63%; 21.0%) were well below the threshold. *B. ayatagriensis* RMG6^T also showed relatively high values (ANIb 97.58%; dDDH 80.0%), above the species threshold. Differences in G + C content between the isolate and the reference genomes were small for all closely related strains (≤ 0.27%), and larger only for *B. nakamurai* (1.10%) and *B. tequilensis* (2.38%).

Table 2
Genomic relatedness to selected *Bacillus* strains

Reference strain	ANIb (%)	dDDH d4 (%)	ΔG + C (%)
B. velezensis FZB42[1]	98.76	91.1	0.12
B. velezensis KACC 18228T[1]	98.56	88.8	0.08
B. velezensis KACC 13105[1]	98.15	84.5	0.07
B. velezensis NRRL B-41580T	98.06	84.2	0.04
B. ayatagriensis RMG6T	97.58	80.0	0.27
B. siamensis KCTC 13613T	93.97	56.8	0.02
B. amyloliquefaciens DSM 7T	93.31	55.1	0.27
B. nakamurai NRRL B-41091T	85.48	30.8	1.10
B. tequilensis NCTC13306T	76.63	21.0	2.38

The genome-scale phylogeny (Fig. 1) placed the isolate within a clade comprising the *B. velezensis reference* strains and B. ayatagriensis RMG6^T (support 83%), where it formed a sister lineage to strain FZB42. A separate clade comprised *B. siamensis* KCTC 13613 and *B. vanillae* XY18 (76%), while *B. amyloliquefaciens* DSM 7 was more distant, and *B. nakamurai* and *B. tequilensis* were the most divergent. Together with the dDDH and ANIb values, these results identify the isolate as a member of *B. velezensis*; the inclusion of *B. ayatagriensis* RMG6^T within the same species cluster indicates that species boundaries in this group should be interpreted with care.

3.2. Functional landscape and genomic architecture

The circular genome map summarizes the genomic organization of the isolate, including protein-coding sequences, tRNA, rRNA, tmRNA, ncRNA, and regulatory elements, together with GC skew across the assembled contigs (Fig. 2). Of the predicted protein-coding genes, 3,624 were assigned to an eggNOG ortholog, and 3,416 of these received a COG category, 2,333 a KEGG Orthology (KO) identifier, 1,063 an EC number, and 1,033 at least one GO term.

Among the COG categories, "Function unknown" (S) was the largest group (936 genes; 27.4% of COG-assigned genes), indicating that a considerable part of the proteome remains uncharacterized (Fig. 3A). Among categories with assigned functions, amino acid transport and metabolism (E; 328 genes), transcription (K; 312), carbohydrate transport and metabolism (G; 249), and inorganic ion transport and metabolism (P; 231) were the most abundant, followed by cell wall/membrane/envelope biogenesis (M) and energy production and conversion (C), with 204 genes each. Signal transduction mechanisms (T) accounted for 154 genes, and defense mechanisms (V) for 59.

KEGG pathway assignment placed the largest number of proteins in ABC transporters (125), two-component systems (123), biosynthesis of amino acids (122), and carbon metabolism (106), followed by quorum sensing (81) and purine metabolism (74) (Fig. 3B). Pathways of central carbohydrate metabolism, including glycolysis/gluconeogenesis (49), pyruvate metabolism (45), amino sugar and nucleotide sugar metabolism (45), and starch and sucrose metabolism (38), were also well represented.

GO annotation was dominated by small-molecule biosynthetic process (123), transport (119), and response to stimulus (102) in the biological process category (Fig. 3C). Cytoplasm (329) and plasma membrane (199) were the most frequent cellular components. Within molecular function, transferase (185), hydrolase (136), transporter (102), and oxidoreductase (81) activities were the most represented. Together, the high representation of transport, signal transduction, and carbohydrate metabolism, along with a substantial set of hydrolases and oxidoreductases, indicates a genome equipped for nutrient uptake, environmental sensing, and diverse substrate conversion.

3.3. Comparative genomics reveals core, accessory, and isolate-associated features

Pan-genome analysis of the marine isolate and four reference *B. velezensis* genomes (B41580, FZB42, KACC 13105, and KACC 18228) grouped 4,303 orthologous gene clusters. Of these, 3,375 (78.4%) were shared by all five genomes (core genome), and the remaining 928 (21.6%) formed the accessory genome (Fig. 4A). The marine isolate carried 3,723 gene clusters, of which 3,375 were core, 272 were shared accessory, and 76 were isolate-specific. The number of genome-specific clusters in the marine isolate (76) fell within the range of the reference strains (71–153), indicating that it is not unusually divergent in gene content.

The UpSet plot (Fig. 4B) showed that, after the core set, the largest intersections were genome-specific sets, led by B41580 (153), KACC 13105 (96), KACC 18228 (79), the marine isolate (76), and FZB42 (71). Among the accessory intersections, the marine isolate shared most clusters with KACC 18228 (177) and FZB42 (173), followed by B41580 (149) and KACC 13105 (141). A further 42 clusters were present in all four reference genomes but absent from the marine isolate.

Functional examination of the 76 isolate-specific clusters indicated that most had no clear metabolic role. Of these, 43 were located in two blocks of consecutive genes containing mobile-element-associated genes (the recombinase xerC, immA/immR, rapG/rapI, and phage-like ribonucleases), based on their genomic position. Three encoded restriction–modification components (hsdR, a Type-II restriction enzyme, and the methylase haeIIIM), and three were other annotated genes (rapG, cdiI, bcrA). The remaining 27 were hypothetical proteins outside these blocks. Only two clusters pointed to a possible environmental function: olsG (ornithine lipid N-methyltransferase) and cwlH (cell-wall amidase), both located within mobile-associated regions. Overall, the isolate-specific gene content was dominated by mobile genetic elements, whereas most of the gene repertoire was shared with the reference genomes.

3.4. Genomic reconstruction reveals mannitol biosynthetic potential

Genome reconstruction identified a mannitol-related metabolic module in the isolate, but only part of a complete biosynthetic route (Fig. 5A; Table 3). A PTS-type uptake system was encoded by mtlA (LOCUS_10390, EIICB component) and mtlF (LOCUS_10400, EIIA component), which were annotated as mannitol-specific enzyme II components (EC 2.7.1.197) and matched their *B. velezensis* FZB42 seed orthologs at 100% and 99.3% identity, respectively. Immediately downstream, mtlD (LOCUS_10410) encoded mannitol-1-phosphate 5-dehydrogenase (EC 1.1.1.17; KO K00009), which catalyses the reversible interconversion of mannitol-1-phosphate (M1P) and fructose-6-phosphate. The MtlD protein contained both the N-terminal Mannitol_dh and C-terminal Mannitol_dh_C domains and showed 97.9% identity to its seed ortholog and 98.39% identity to the *B. velezensis* protein WP_224443509.1 in BLASTp. A predicted transcriptional regulator of the mannitol operon, mtlR (LOCUS_10560), was located 15 genes downstream of mtlD. The gene immediately upstream of mtlA encoded a DeoR-type regulator, which was annotated as the copper-responsive regulator YcnK and clustered with copper-related genes, and was therefore not considered part of the mannitol module (Fig. 5B).

By contrast, genes for the subsequent steps toward free mannitol were not detected. No gene was assigned to mannitol-1-phosphatase (M1Pase; EC 3.1.3.22), which would dephosphorylate M1P, nor to mannitol 2-dehydrogenase (EC 1.1.1.67 or 1.1.1.138), which would reduce fructose directly to mannitol (Fig. 5A). Candidate phosphatases were therefore selected from the genome on the basis of their likelihood to act as sugar-phosphate phosphatases (Table 3). Six HAD-superfamily proteins met this criterion: LOCUS_10440 (ycsE), LOCUS_25690 (araL), LOCUS_18400 and LOCUS_18410 (supH), LOCUS_25540 (ysaA), and LOCUS_15180 (ykrA). All six carried the HAD catalytic motif I (DxDx[T/V]), and four of them (LOCUS_10440, LOCUS_15180, LOCUS_18400, and LOCUS_18410) also carried the Cof-type motif IV (GDxxND). Their seed orthologs were highly similar (96.7–100% identity), and none was annotated as M1Pase. The EC number assigned by eggNOG to LOCUS_10440 was 3.1.3.104 (sucrose-6F-phosphate phosphohydrolase), not 3.1.3.22.

Table 3
Genes of the mannitol metabolic module identified in the marine *B. velezensis* genome

Locus tag	Gene	Role	Seed Ortholog
LOCUS_10390	mtlA	PTS mannitol-specific EIICB component; mannitol uptake and phosphorylation to M1P (EC 2.7.1.197)	RBAM_004230
LOCUS_10400	mtlF	PTS mannitol-specific EIIA component (EC 2.7.1.197)	RBAM_004240
LOCUS_10410	mtlD	Mannitol-1-phosphate 5-dehydrogenase; M1P ⇌ fructose-6-phosphate (EC 1.1.1.17)	RBAM_004250
LOCUS_10560	mtlR	Transcriptional regulator of the mannitol operon (predicted)	RBAM_004390
LOCUS_10440	ycsE	HAD-family phosphatase; candidate M1P phosphatase (putative)	RBAM_004270
LOCUS_25690	araL	HAD-family sugar phosphatase (putative)	RBAM_025830
LOCUS_18400	supH	Cof-type HAD-IIB sugar phosphatase (putative)	RBAM_024170
LOCUS_18410	supH	HAD-IIB hydrolase (putative)	RBAM_024160
LOCUS_25540	ysaA	HAD-family hydrolase (putative)	RBAM_025980
LOCUS_15180	ykrA	Cof-type HAD-IIB hydrolase (putative)	RBAM_014290

Note: Seed orthologs were assigned by eggNOG-mapper against B. velezensis FZB42 (taxon 326423; RBAM_ locus tags). "Putative" indicates annotation-based candidates for the mannitol-1-phosphatase step (EC 3.1.3.22), which was not detected.

Genomic context favored two of the candidates (Fig. 5B). LOCUS_10440 lay three genes downstream of mtlD, between genes encoding FabZ and a hypothetical protein, whereas LOCUS_25690 was located in an arabinose-utilization region together with L-arabinose isomerase, ribulokinase, and L-ribulose-5-phosphate 4-epimerase. LOCUS_18400 and LOCUS_18410 flanked a mannose-6-phosphate isomerase and an RpiR-family regulator, and LOCUS_25540 and LOCUS_15180 were located in genomic contexts without apparent links to sugar metabolism. All of the genes described above, including the six candidates, were present in all five genomes included in the pan-genome analysis. Taken together, the isolate encodes the PTS uptake system and MtlD, whereas the phosphatase step required for mannitol formation could be assigned only to putative HAD-family candidates without direct evidence of M1P hydrolysis. The mannitol biosynthetic capacity of the isolate should therefore be regarded as putative.

3.5. Detection of trace mannitol in glucose- and fructose-supplemented cultures

Mannitol was detected in the culture supernatants of the isolate after 42 h of fermentation with glucose or fructose, but only at low concentrations (Fig. 6). The mannitol calibration curve was linear over 0–100

mg/L (R^2 = 0.9989), and the concentrations measured in the samples fell within this range. The glucose-supplemented culture contained 44.70 ± 1.25 mg/L mannitol, and the fructose-supplemented culture contained 63.96 ± 1.11 mg/L (mean ± SD, n = 3).

Mannitol was identified by the retention time of the authentic standard, but it elutes close to fructose and mannose in the chromatographic system used. These values therefore indicate that low levels of mannitol are present in the cultures, but they do not establish mannitol production by the isolate. The detection of mannitol is compatible with the presence of the mtl module, and its low concentration may be compatible with the absence of an annotated mannitol-1-phosphatase. The mannitol biosynthetic capacity of the isolate should therefore remain regarded as putative.

3.6. Comparative genomics reveals a conserved repertoire of salinity- and stress-adaptive systems

Targeted comparison of the marine isolate with the four reference genomes showed that it carries a broad repertoire of systems associated with coping with saline and fluctuating environments (Table 4). For osmotic adjustment, the genome encodes uptake systems for glycine betaine and related compatible solutes (OpuA and OpuC), the glycine betaine synthesis genes gbsB and betB, and the proline biosynthesis genes proB and proC. Ion homeostasis was supported by the potassium transporters KtrC, KimA, and TrkH and by several Na^+/H^+ antiporters (Nha/Mnh, NhaC, and NhaK), while the mechanosensitive channel MscL and the MscS-family protein YfkC were also present. General stress responses were represented by the σB module (SigB and RsbW), the extracytoplasmic function sigma factors SigM, SigW, and SigX, the protease ClpP, the chaperonins GroEL and GroES, and the cold-shock proteins CspB, CspC, and CspD. Genes related to membrane fluidity (the desaturase gene desA and the regulator desR), oxidative stress defence (KatA, SodA, and AhpC/AhpF), and biofilm formation (TasA, BslB, and SinR) were also identified.

Table 4
Salinity- and stress-adaptive systems across the five genomes

System	Components	Locus tags	Genomes with ortholog
Compatible solutes	OpuA (opuAA, opuAB)	LOCUS_01120, LOCUS_01130	5/5
Compatible solutes	OpuC (opuCB, opuCD)	LOCUS_35870, LOCUS_35850	5/5
Compatible solutes	Glycine betaine synthesis (gbsB, betB)	LOCUS_21130, LOCUS_21120	5/5
Compatible solutes	Proline synthesis (proB, proC)	LOCUS_06440, LOCUS_23920	5/5
Potassium	KtrC; KimA; TrkH	LOCUS_15140, LOCUS_10710, LOCUS_14140	5/5
Na+/H+	Nha/Mnh (nha, mrpF, nhaC, nhaK)	LOCUS_20560, LOCUS_20520, LOCUS_12460, LOCUS_35370	5/5
Mechanosensitive	MscL; YfkC (MscS-family)	LOCUS_07860, LOCUS_29110	5/5
General stress	σB (sigB, rsbW)	LOCUS_32280, LOCUS_32290	5/5
General stress	ECF σ (sigM, sigW, sigX)	LOCUS_36930, LOCUS_00190, LOCUS_12910	5/5
General stress	ClpP; GroEL/GroES	LOCUS_02670, LOCUS_13810, LOCUS_13820	5/5
General stress	Cold shock (cspB, cspC, cspD)	LOCUS_37320, LOCUS_31800, LOCUS_25260	5/5
General stress	Membrane fluidity (desA, desR)	LOCUS_31810, LOCUS_30080	5/5
Oxidative stress	KatA; SodA; AhpC/AhpF	LOCUS_37610, LOCUS_35150, LOCUS_30190, LOCUS_30200	5/5
Biofilm	TasA; BslB; SinR	LOCUS_36530, LOCUS_21100, LOCUS_36520	5/5

All these systems were present in all five genomes, with one exception: desA was absent from B41580 and KACC18228. The adaptive repertoire of the marine isolate therefore appears to be largely conserved within the group rather than restricted to this strain. This conservation is consistent with the capacity of the isolate to tolerate saline conditions, although the genomic data alone do not demonstrate it, and it should be confirmed experimentally.

Beyond the genes listed in Table 4, the annotation indicated additional routes for compatible-solute handling. For proline, proA was present together with two copies each of proB and proC, as well as

comER. For glycine betaine, opuD and a second OpuC cluster (opuCA–CD) were annotated in addition to the uptake and synthesis genes in Table 4, and trehalose utilization genes (treP, treC, and treR) were present. The glutamate-related genes gltA, gltD, and glnA may supply precursors for these pathways. Genes for opuB, opuE, ectABC, and otsAB were not annotated, so ectoine synthesis and trehalose biosynthesis via OtsAB could not be inferred. Together, these annotations indicate a capacity for proline synthesis and glycine betaine uptake and synthesis, while the use of other compatible solutes is not supported by the annotation.

3.7. Genome mining reveals conserved antimicrobial biosynthetic clusters

antiSMASH analysis predicted 18 biosynthetic gene clusters (BGCs) in the genome of the marine isolate (Table 5). The regions were dominated by nonribosomal peptide synthetase (NRPS) and polyketide synthase (PKS) clusters, with eight regions containing NRPS and eight containing PKS-type modules (trans-AT PKS, type III PKS, or PKS-like), including hybrid regions. In addition, two terpene regions, two ribosomally synthesized and post-translationally modified peptide (RiPP) regions, and one region classified as "other" were detected.

Table 5
Biosynthetic gene clusters predicted by antiSMASH in the marine isolate

Region	Type	Most similar known cluster	Similarity
5.1 †	NRPS	Surfactin	47%
7.1 †	NRPS	Plipastatin	30%
8.1	Terpene	–	–
16.1 †	trans-AT PKS	Difficidin	46%
18.1 †	trans-AT PKS-like	Difficidin	53%
19.1 †	NRPS	Surfactin	17%
21.1 †	NRPS	Fengycin	20%
23.1	trans-AT PKS	Macrolactin H	100%
25.1 †	NRPS	Fengycin	20%
29.1	Terpene	–	–
30.1	RiPP-like, NRPS	Bacillibactin	100%
31.1 †	NRPS, betalactone, trans-AT PKS	Fengycin	80%
31.2	trans-AT PKS, NRPS, T3PKS	Bacillaene	100%
34.1 †	T3PKS	–	–
38.1	LAP, RRE-containing	Plantazolicin	91%
42.1 †	trans-AT PKS-like	Difficidin	26%
45.1	Other	Bacilysin	100%
49.1 †	PKS-like	–	–

† Region located at a contig edge and possibly incomplete.

Five regions matched characterized clusters in the MIBiG database with high similarity: macrolactin H (region 23.1, 100%), bacillibactin (30.1, 100%), bacillaene (31.2, 100%), bacilysin (45.1, 100%), and plantazolicin (38.1, 91%). Region 31.1 showed 80% similarity to the fengycin cluster. The remaining NRPS and trans-AT PKS regions showed partial similarity to the surfactin, plipastatin/fengycin, and difficidin clusters (17–53%). Most of these partial matches (regions 5.1, 7.1, 16.1, 18.1, 19.1, 21.1, 25.1, and 42.1) were located at contig edges, which suggests that these clusters may be split across contigs in the current assembly. Four regions (8.1, 29.1, 34.1, and 49.1) showed no similarity to known clusters and may represent uncharacterized candidates. Overall, the repertoire is consistent with the biosynthetic potential commonly associated with Bacillus velezensis, although the production of these metabolites remains to be experimentally verified.

3.8. Cell wall hydrolytic machinery and remodelling dynamics

The genome encodes a broad set of putative peptidoglycan-active enzymes (Fig. 7, provisional numbering). dbCAN3 assigned glycoside hydrolases from families GH73 (three proteins), GH23 (five), GH18 (two), GH46, and GH171 to cell wall–related functions, together with six carbohydrate esterases of family CE4 and eleven proteins carrying LysM (CBM50) modules. Most of these proteins have a modular organization. The LysM proteins LytE and LytF carry two and five N-terminal LysM repeats, respectively, and preceded by a signal peptide. Two GH18 proteins carry LysM modules or a LysM-containing region, and the GH73 protein LytD is a large protein of 881 amino acids with a signal peptide and a C-terminal catalytic module.

Beyond these families, eggNOG annotation indicated further cell wall–modifying enzymes: eleven N-acetylmuramoyl-L-alanine amidases, including LytC, LytH, CwlC, CwlJ, and SleB; eight proteins with NlpC/P60 domains; and six D,D-carboxypeptidases (DacA, DacB, DacC, DacF, YodJ, and one unnamed). Six CE4 polysaccharide deacetylases, five of them with a predicted signal peptide, may be involved in peptidoglycan modification. Some of these genes are associated with sporulation (sleB, cwlJ, spoVID) or with prophage regions (xlyA, xlyB), so not all of them are expected to act in vegetative growth. These assignments rest on family-level annotation, and their activity and role in cell wall turnover have not been tested.

3.9. Fermentative metabolic pathways and aroma precursor biosynthesis

Annotation of the genome identified the core enzymes of several fermentative and precursor-supplying pathways (Fig. 8; locus tags in Supplementary **Table S2**). From pyruvate, genes for lactate dehydrogenase (ldh), the pyruvate dehydrogenase complex (pdhABCD), and acetolactate synthase (alsS) were present. The acetoin branch was complete at the annotation level: alsS and acetolactate decarboxylase (alsD) were encoded in adjacent loci, together with an acetoin/2,3-butanediol dehydrogenase (bdhA) and the acetoin dehydrogenase complex (acoABCL) with its regulator acoR. Phosphotransacetylase (pta) and acetate kinase (ackA) indicate the potential to form acetate, and several alcohol dehydrogenases (adhP, adhB, adhA) were also annotated. A pyruvate-formate lyase (pflB), a bifunctional alcohol/aldehyde dehydrogenase (adhE), and a pyruvate decarboxylase were not annotated, so the route to ethanol could not be resolved.

Genes for the supply of aroma-related precursors were also found. The branched-chain amino acid pathway (ilvBN, ilvC, ilvD, ilvE, and leuABCD) was annotated, and a bkd gene cluster encoding a branched-chain α-keto acid dehydrogenase complex lay next to ptb and buk, which may link branched-chain amino acid catabolism to branched-chain short-chain acids. The shikimate pathway and the terminal steps to phenylalanine, tyrosine, and tryptophan (pheA, tyrA, trpEDCFBA) were annotated. Aldehyde dehydrogenases and a phenolic acid decarboxylase (padC) were also present. No

phenylpyruvate decarboxylase was annotated, so a direct Ehrlich-type route from phenylpyruvate to 2-phenylethanol cannot be inferred from this dataset. These annotations indicate genomic potential only. Whether the isolate produces acetoin, 2,3-butanediol, or other volatile compounds must be tested experimentally.

4. Discussion

This study combined taxonomic, pan-genomic and functional analyses of a *Bacillus velezensis* isolate from barnacle biofilm, with emphasis on mannitol metabolism and on traits that may support life in a marine, surface-attached habitat. Three findings frame the discussion. The isolate is a typical member of the species in gene content, and its small isolate-specific fraction is dominated by mobile genetic elements. It encodes the uptake and dehydrogenase steps of mannitol metabolism but no annotated mannitol-1-phosphatase, and only low levels of mannitol were measured in culture. Finally, its osmoadaptive, biosynthetic, cell wall and fermentative repertoires are rich but largely shared with the reference genomes. The interest of the isolate therefore lies less in unique genes than in how a conserved toolkit is deployed, and in a single missing metabolic step.

Genome-based indices place the isolate clearly within *B. velezensis*. Its ANIb values (98.06–98.76%) and dDDH values (84.2–91.1%) against the four reference genomes exceed the thresholds of approximately 95% ANI (Jain et al., 2018) and 70% dDDH, which agrees with the reclassification of *B. amyloliquefaciens subsp. plantarum*, *B. methylotrophicus* and *B. oryzicola* as later heterotypic synonyms of *B. velezensis* (Dunlap et al., 2016). *B. siamensis* and *B. amyloliquefaciens* DSM 7^T fell below these thresholds, in line with the separation of these taxa within the “operational group B. amyloliquefaciens” (Fan et al., 2017). One result deserves comment. *B. ayatagriensis* RMG6T was described as closest to *B. siamensis* (94.44% OrthoANIu; 56.80% dDDH), and its description reports no comparison with *B. velezensis* (Das et al., 2025). Relative to our isolate, however, it lay above the species thresholds (97.58% ANIb; 80.0% dDDH). We draw no taxonomic conclusion from a single comparison, but the discrepancy suggests that the boundaries of this species complex deserve re-examination with denser genome sampling. Because no 16S rRNA gene could be recovered from the short-read assembly, species assignment rests entirely on genome-wide indices.

The pan-genome analysis should be read in light of how pan-genomes behave. In an open pan-genome, the number of gene families keeps increasing as genomes are added, and the core genome shrinks accordingly, whereas a closed pan-genome reaches a plateau. The *B. subtilis* group is characterized by open pan-genomes (Wang et al., 2024), and larger *B. velezensis* datasets illustrate the trend. A comparison that included B. velezensis strains reported 3,135 core and 864 accessory genes among 20 strains (Zeng et al., 2025), and a dataset of 271 genomes reported only about 16% core genes (Bach et al., 2025). The core of 3,375 of 4,303 gene clusters (78.4%) that we found therefore reflects five genomes and strict-mode clustering (Tonkin-Hill et al., 2020), not a species-level estimate, and it would be expected to shrink as genomes are added. Within this limited frame, the 76 isolate-specific clusters fell within the range of the reference strains (71–153), and most were hypothetical or located in blocks

carrying recombinase, phage-like and restriction–modification genes. This agrees with reports that prophages and genomic islands are major sources of accessory content in *B. velezensis* (Xu et al., 2020; Ma and Hu, 2019; Hu et al., 2025). The two isolate-specific genes with a conceivable environmental role, olsG and cwlH, lay within such regions, so we cannot link them to the marine habitat, and their placement should be confirmed with long reads.

The isolate carries an mtlAFD arrangement with a candidate mtlR regulator that parallels the organization of the *B. subtilis* mannitol system, in which MtlD is required for growth on mannitol and MtlR controls the operon through PTS-dependent phosphorylation. We did not test whether MtlD is required for growth on mannitol in the isolate, but the arrangement points first to a catabolic function. This would be unsurprising for a marine isolate, because mannitol is a major storage compound of algae and a marine carbon source (Tonon et al., 2017; Xiao et al., 2024). All mannitol-related genes, including the six phosphatase candidates, were present in all five genomes, so the module is a species-level feature and not an adaptation of this isolate.

Formation of free mannitol additionally requires dephosphorylation of mannitol-1-phosphate. Without it, MtlD would only interconvert mannitol-1-phosphate and fructose-6-phosphate, and the PTS could re-import any free mannitol that appeared outside the cell. This step has been supplied heterologously in engineered mannitol producers (Madsen et al., 2018), and brown algal mannitol-1-phosphatases carry it out with high specificity (Le Strat et al., 2023). We found no annotated mannitol-1-phosphatase and nominated six HAD-superfamily phosphatases as candidates on the basis of catalytic motifs and genomic context. This evidence is circumstantial. Motif I, and the Cof-type motif IV in four candidates, indicate fold and mechanism but not substrate, and HAD enzymes of B. subtilis can accept broad ranges of substrates (Zakataeva et al., 2016; Terakawa et al., 2016). Functions transferred by annotation are also error-prone (Price et al., 2018; Danchin et al., 2018), as illustrated by the EC number 3.1.3.104 that eggNOG-mapper assigned to LOCUS_10440. Mannitol was nonetheless detected in culture supernatants, at 44.70 ± 1.25 mg/L with glucose and 63.96 ± 1.11 mg/L with fructose. This is compatible with dephosphorylation of mannitol-1-phosphate by one of the candidate phosphatases, but it is equally compatible with other routes, such as unannotated dehydrogenase activities, mannitol present in the medium components, or analytical overlap, and it does not by itself identify the responsible enzyme or whether the mannitol detected in the supernatant was exported or released by cell lysis. Because annotation is incomplete, the lack of an annotated mannitol-1-phosphatase does not exclude the activity, and the six candidates are the most plausible genomic sources of the missing step. They are therefore potential routes to free mannitol, not demonstrated ones. The measurements also need cautious reading. Mannitol elutes close to fructose and mannose under the chromatographic conditions used and was identified by retention time alone. MRS medium already contains 20 g/L dextrose, so the 100 mg/L of added glucose or fructose is a small fraction of the available sugar, and the difference between the two supplements, which was not tested statistically, should not be interpreted as a substrate effect. These values are therefore preliminary, and they show that mannitol can be detected, not that a defined enzyme forms it. Mannitol is an industrially relevant polyol (Chen et al., 2020; Zhang et al., 2018), and the question has been reduced to a single, tractable step. Testing the recombinant candidates with mannitol-

1-phosphate and other sugar phosphates would show whether any of them has this activity, and until then the mannitol route of the isolate remains putative.

The osmoadaptive repertoire of the isolate resembles the well-studied B. subtilis response, which combines uptake and synthesis of compatible solutes, potassium homeostasis and mechanosensitive channels (Hoffmann and Bremer, 2016; Bremer and Krämer, 2019). Proline synthesis and glycine betaine handling are central to this response (Hoffmann et al., 2017; Stecker et al., 2022), and the potassium transporter KimA, which is controlled by cyclic di-AMP, links ion homeostasis to osmolyte transport (Gundlach et al., 2019; Commichau et al., 2018). With the single exception of desA, all of these systems were present in all five genomes. Because the core genome of an open pan-genome shrinks as genomes are added, conservation across five genomes does not prove universality, but it does indicate that the toolkit is not restricted to this isolate. Other genome studies of *B. velezensis* from seaweed and coastal seawater give a mixed picture. Hyperosmotic-stress gene clusters were conserved across strains in a seaweed-associated isolate (Vairagkar et al., 2021), whereas a coastal strain was reported to carry strain-specific genes enriched in marine-adaptation functions (Lin et al., 2026). The outcome probably depends on the comparator set. *B. velezensis* QA2 has been reported to grow in up to 11% NaCl on solid medium (Mahdi et al., 2022), which is consistent with a generalist rather than a marine specialist. If habitat adaptation exists, it may lie in regulation, as suggested by regulatory mutations arising during salinity-driven evolution of a related strain (Goszcz et al., 2026), but this cannot be tested without expression data. The annotation also limits what can be said about other compatible solutes. Genes for ectoine synthesis were not annotated, although ectoine synthesis is widespread among bacteria (Czech et al., 2018), so the isolate appears to rely on proline and glycine betaine, and this does not demonstrate tolerance to any particular salinity.

Genes for matrix formation, including tasA and the repressor sinR, were also present, which is consistent with the central role of these components in Bacillus biofilms (Arnaouteli et al., 2021). Whether such an isolate influences barnacle settlement cannot be inferred from the genome, and the available evidence is not consistent. A B. licheniformis extract had low efficacy against *Amphibalanus amphitrite* settlement (Muras et al., 2021), whereas biosurfactant-producing marine bacteria reduced biofilm formation and biofouling in other assays (Alemán-Vega et al., 2020). Our data show only that the genetic basis for biofilm formation is present.

antiSMASH predicted 18 regions, and five matched characterized clusters at 91–100% similarity (macrolactin H, bacillibactin, bacillaene, bacilysin and plantazolicin). These products belong to the classical secondary metabolome of *B. velezensis* and of its model strain FZB42 (Fan et al., 2018), and the distribution of such clusters across the B. subtilis species complex has been mapped in detail (Steinke et al., 2021; Zeng et al., 2025). The lower similarity values (17–53%) need careful reading. Eleven of the 18 regions lay at contig edges, and the partial matches to surfactin, plipastatin/fengycin and difficidin were concentrated among them. Long, repetitive NRPS and PKS genes are split across contigs in short-read assemblies (Meleshko et al., 2019; Tizabi et al., 2022; Sánchez-Navarro et al., 2022), so low scores more probably indicate incomplete clusters than divergent ones and should not be

read as novelty. Likewise, two of the four regions without similarity to known clusters were at contig edges, and a newer version of antiSMASH is available (Blin et al., 2023). None of the clusters has been shown to be expressed. Their relevance to the habitat remains a hypothesis, because lipopeptides of *B. velezensis* have been implicated in interference competition against marine bacteria (Cai et al., 2026), and a sponge-associated strain also carries several clusters with little similarity to known ones (Devkar et al., 2025), but neither observation was tested here.

The cell wall hydrolase set resembled that of the model organism. LytE and LytF carry LysM repeats and an annotated NlpC/P60 domain, which is the organization expected of D,L-endopeptidases acting on peptidoglycan (Egan et al., 2020). In B. subtilis, D,L-endopeptidase activity is essential for growth (Hashimoto et al., 2018), CwlO acts together with the FtsEX complex and its cofactors (Brunet et al., 2019), and the WalRK system adjusts the activity of CwlO and LytE (Dobihal et al., 2019). Several other genes belong to spore germination or prophage lysis and are not expected to act in vegetative growth. The GH18 and GH46 families can include chitinases and chitosanases of biocontrol relevance (Tran et al., 2022; Cui et al., 2021). Family-level assignment cannot, however, distinguish remodeling of the bacterium's own wall from degradation of external substrates, so function must be tested.

The fermentative annotation was complete for the acetoin and 2,3-butanediol branch (alsS, alsD, bdhA and acoABCL) and for lactate and acetate formation, whereas pflB and adhE were absent, so the route to ethanol remains unresolved. Acetoin and 2,3-butanediol have reached high titres in *B. amyloliquefaciens* (Petrov and Petrova, 2021), and acetoin is a precursor of tetramethylpyrazine and of the pyrazines that characterize Bacillus-fermented soybean products (Li et al., 2023; Guo et al., 2024; Yi and Hong, 2021). No phenylpyruvate decarboxylase was annotated, so a direct Ehrlich-type route to 2-phenylethanol cannot be inferred, and bacterial 2-phenylethanol production has generally required a heterologous decarboxylase such as yeast Aro10 (Zhu et al., 2023; Bernardino et al., 2024). These traits are typical of the genus and represent genomic potential that depends on growth conditions.

Several limitations bound these conclusions. The analysis rests on one isolate and a 49-contig Illumina assembly, in which fragmented clusters and mobile regions may be misrepresented. The pan-genome included only five genomes, and about 27% of COG-assigned genes had unknown function, so functional assignments rely on transferred annotation, a recognized source of error (Price et al., 2018; Danchin et al., 2018). Only one phenotype, low-level mannitol, was measured, with limited controls, and salt tolerance, antimicrobial activity and fermentation products were not. The next experiments follow directly from the findings and include (i) a mannitol-specific assay and uninoculated controls, together with measurements under different NaCl concentrations; (ii) expression of the six HAD candidates and assays with mannitol-1-phosphate and other sugar phosphates; (iii) measurement of mtl and candidate gene expression under salt stress; (iv) long-read sequencing to close the biosynthetic regions; and (v) growth and settlement assays comparing the isolate with the reference strain

Declarations

Declaration of competing interest

The authors declare that they have no known competing financial interests or personal relationships that could have appeared to influence the work reported in this paper.

Funding

This work was supported by the Ministry of Higher Education, Science, and Technology of the Republic of Indonesia (Kemdiktisaintek) through the Pendidikan Magister menuju Doktor untuk Sarjana Unggul (PMDSU) scheme, Penelitian Lanjutan 2026, under contract number 077/C3/DT.05.00/PL-MULTITAHUN LANJUTAN/2026.

Author Contribution

A.A., H.H. and M.S. conceived the study. N.B. performed the investigation, prepared the figures and wrote the original draft of the manuscript. M.Y. curated the data. H.A.M. reviewed and edited the manuscript. H.H. acquired the funding. M.Y., I.M.H., A.A., H.H. and M.S. supervised the work. All authors reviewed and approved the final manuscript.

Acknowledgement

The authors thank the COI-NEXT project at Tokyo University of Agriculture and Technology (TUAT), and especially the Department of Life Science, for facilitating the training and learning that made this work possible.

References

1. Alemán-Vega M, Sánchez-Lozano I, Hernández-Guerrero CJ et al (2020) Exploring antifouling activity of biosurfactants producing marine bacteria isolated from Gulf of California. Int J Mol Sci 21:6068. https://doi.org/10.3390/ijms21176068
2. Arnaouteli S, Bamford NC, Stanley-Wall NR, Kovács ÁT (2021) *Bacillus subtilis* biofilm formation and social interactions. Nat Rev Microbiol 19:600–614. https://doi.org/10.1038/s41579-021-00540-9
3. De Bacchetti T, Khandeparker L, Anil AC, Mesbahi E, Burgess JG, Clare AS (2012) Characterisation of the bacteria associated with barnacle, *Balanus amphitrite*, shell and their role in gregarious settlement of cypris larvae. J Exp Mar Biol Ecol 413:7–12. https://doi.org/10.1016/j.jembe.2011.11.014
4. Bach E, Ritter AC, Silveira RD et al (2025) Pangenome analysis of *Bacillus velezensis* exploring the probiotic potential and plant growth promotion traits of strains isolated from fish intestines. Mol Genet Genomics 300:20. https://doi.org/10.1007/s00438-025-02230-0

5. Bernardino ARS, Torres CAV, Crespo JG, Reis MAM (2024) Biotechnological 2-phenylethanol production: recent developments. Molecules 29:5761. https://doi.org/10.3390/molecules29235761
6. Blin K, Shaw S, Kloosterman AM et al (2021) antiSMASH 6.0: improving cluster detection and comparison capabilities. Nucleic Acids Res 49:W29–W35. https://doi.org/10.1093/nar/gkab335
7. Blin K, Shaw S, Augustijn HE et al (2023) antiSMASH 7.0: new and improved predictions for detection, regulation, chemical structures and visualisation. Nucleic Acids Res 51:W46–W50. https://doi.org/10.1093/nar/gkad344
8. Bremer E, Krämer R (2019) Responses of microorganisms to osmotic stress. Annu Rev Microbiol 73:313–334. https://doi.org/10.1146/annurev-micro-020518-115504
9. Brunet YR, Wang X, Rudner DZ (2019) SweC and SweD are essential co-factors of the FtsEX-CwlO cell wall hydrolase complex in *Bacillus subtilis*. PLoS Genet 15:e1008296. https://doi.org/10.1371/journal.pgen.1008296
10. Byer T, Wang J, Zhang MG, Vather N, Blachman A, Visser B, Liu JM (2017) MtlR negatively regulates mannitol utilization by *Vibrio cholerae*. Microbiology 163:1902–1911. https://doi.org/10.1099/mic.0.000559
11. Cai R, Feng H, Liu Y et al (2026) Surfactin-like lipopeptides contribute to interference competition of *Bacillus velezensis* against the marine Flavobacteriaceae in phycosphere. Environ Microbiome. https://doi.org/10.1186/s40793-026-00937-0
12. Chen M, Zhang W, Wu H, Guang C, Mu W (2020) Mannitol: physiological functionalities, determination methods, biotechnological production, and applications. Appl Microbiol Biotechnol 104:6941–6951. https://doi.org/10.1007/s00253-020-10757-y
13. Commichau FM, Gibhardt J, Halbedel S, Gundlach J, Stülke J (2018) A delicate connection: c-di-AMP affects cell integrity by controlling osmolyte transport. Trends Microbiol 26:175–185. https://doi.org/10.1016/j.tim.2017.09.003
14. Cui D, Yang J, Lu B et al (2021) Efficient preparation of chitooligosaccharide with a potential chitosanase Csn-SH and its application for fungi disease protection. Front Microbiol 12:682829. https://doi.org/10.3389/fmicb.2021.682829
15. Czech L, Hermann L, Stöveken N et al (2018) Role of the extremolytes ectoine and hydroxyectoine as stress protectants and nutrients: genetics, phylogenomics, biochemistry, and structural analysis. Genes 9:177. https://doi.org/10.3390/genes9040177
16. Dai Y, Meng Q, Mu W, Zhang T (2017) Recent advances in the applications and biotechnological production of mannitol. J Funct Foods 36:404–409. https://doi.org/10.1016/j.jff.2017.07.022
17. Danchin A, Ouzounis C, Tokuyasu T, Zucker J-D (2018) No wisdom in the crowd: genome annotation in the era of big data – current status and future prospects. Microb Biotechnol 11:588–605. https://doi.org/10.1111/1751-7915.13284
18. Das S, Mondal R, Mandal P et al (2025) *Bacillus ayatagriensis* sp. nov., a novel plant growth-promoting rhizobacteria strain isolated from mulberry rhizosphere. Sci Rep 15:26693. https://doi.org/10.1038/s41598-025-05508-w

19. Devkar HU, Juyal K, Thakur NL et al (2025) Antimicrobial potential of marine sponge-associated *Bacillus velezensis* and *Stutzerimonas stutzeri* from the Indian coast: a genome mining and metabolite profiling approach. Curr Microbiol 82:280. https://doi.org/10.1007/s00284-025-04262-6
20. Dobihal GS, Brunet YR, Flores-Kim J, Rudner DZ (2019) Homeostatic control of cell wall hydrolysis by the WalRK two-component signaling pathway in *Bacillus subtilis*. eLife 8:e52088. https://doi.org/10.7554/eLife.52088
21. Dunlap CA, Kim SJ, Kwon SW, Rooney AP (2016) *Bacillus velezensis* is not a later heterotypic synonym of *Bacillus amyloliquefaciens*; *Bacillus methylotrophicus*, *Bacillus amyloliquefaciens subsp. plantarum* and '*Bacillus oryzicola*' are later heterotypic synonyms of *Bacillus velezensis* based on phylogenomics. Int J Syst Evol Microbiol 66:1212–1217. https://doi.org/10.1099/ijsem.0.000858
22. Egan AJF, Errington J, Vollmer W (2020) Regulation of peptidoglycan synthesis and remodelling. Nat Rev Microbiol 18:446–460. https://doi.org/10.1038/s41579-020-0366-3
23. Fan B, Blom J, Klenk H-P, Borriss R (2017) *Bacillus amyloliquefaciens*, *Bacillus velezensis*, and *Bacillus siamensis* form an operational group *B. amyloliquefaciens* within the *B. subtilis* species complex. Front Microbiol 8:22. https://doi.org/10.3389/fmicb.2017.00022
24. Fan B, Wang C, Song X et al (2018) *Bacillus velezensis* FZB42 in 2018: the Gram-positive model strain for plant growth promotion and biocontrol. Front Microbiol 9:2491. https://doi.org/10.3389/fmicb.2018.02491
25. Fu H, Yang L, Zhang H, Wang J (2023) Deciphering of the mannitol metabolism pathway in *Clostridium tyrobutyricum* ATCC 25755 by comparative transcriptome analysis. Appl Biochem Biotechnol 195:1072–1084. https://doi.org/10.1007/s12010-022-04209-8
26. Goszcz A, Musiałowski M, Ciuchciński K et al (2026) Salinity-driven evolution of psychrotolerant *Bacillus velezensis* S_51 strain reveals metabolic adaptations to osmotic stress and enhanced glycine betaine production. Microb Cell Fact. https://doi.org/10.1186/s12934-026-03116-5
27. Grembecka M (2015) Sugar alcohols—their role in the modern world of sweeteners: a review. Eur Food Res Technol 241:1–14. https://doi.org/10.1007/s00217-015-2437-7
28. Groisillier A, Labourel A, Michel G, Tonon T (2015) The mannitol utilization system of the marine bacterium *Zobellia galactanivorans*. Appl Environ Microbiol 81:1799–1812. https://doi.org/10.1128/AEM.02808-14
29. Gundlach J, Krüger L, Herzberg C et al (2019) Sustained sensing in potassium homeostasis: cyclic di-AMP controls potassium uptake by KimA at the levels of expression and activity. J Biol Chem 294:9605–9614. https://doi.org/10.1074/jbc.RA119.008774
30. Guo Q, Peng J, He Y (2024) A systematic comparative study on the physicochemical properties, volatile compounds, and biological activity of typical fermented soy foods. Foods 13:415. https://doi.org/10.3390/foods13030415
31. Hashimoto M, Matsushima H, Suparthana IP et al (2018) Digestion of peptidoglycan near the cross-link is necessary for the growth of *Bacillus subtilis*. Microbiology 164:299–307. https://doi.org/10.1099/mic.0.000614

32. Hoffmann T, Bremer E (2016) Management of osmotic stress by *Bacillus subtilis*: genetics and physiology. In: de Bruijn FJ (ed) Stress and environmental regulation of gene expression and adaptation in bacteria. Wiley, Hoboken, pp 657–676. https://doi.org/10.1002/9781119004813.ch63
33. Hoffmann T, Bleisteiner M, Sappa PK et al (2017) Synthesis of the compatible solute proline by *Bacillus subtilis*: point mutations rendering the osmotically controlled *proHJ* promoter hyperactive. Environ Microbiol 19:3700–3720. https://doi.org/10.1111/1462-2920.13870
34. Hopkins G, Davidson I, Georgiades E, Floerl O, Morrisey D, Cahill P (2021) Managing biofouling on submerged static artificial structures in the marine environment – assessment of current and emerging approaches. Front Mar Sci 8:759194. https://doi.org/10.3389/fmars.2021.759194
35. Hu L, Zhang X, Gao Q et al (2025) *Bacillus velezensis* T971 genome informs starch degradation in tobacco. Front Microbiol 16:1689015. https://doi.org/10.3389/fmicb.2025.1689015
36. Ip JC-H, Qiu J-W, Chan BKK (2021) Genomic insights into the sessile life and biofouling of barnacles (Crustacea: Cirripedia). Heliyon 7:e07291. https://doi.org/10.1016/j.heliyon.2021.e07291
37. Iwamoto K, Shiraiwa Y (2005) Salt-regulated mannitol metabolism in algae. Mar Biotechnol 7:407–415. https://doi.org/10.1007/s10126-005-0029-4
38. Jacobsen JH, Frigaard N-U (2014) Engineering of photosynthetic mannitol biosynthesis from CO2 in a cyanobacterium. Metab Eng 21:60–70. https://doi.org/10.1016/j.ymben.2013.11.004
39. Jain C, Rodriguez-R LM, Phillippy AM, Konstantinidis KT, Aluru S (2018) High throughput ANI analysis of 90K prokaryotic genomes reveals clear species boundaries. Nat Commun 9:5114. https://doi.org/10.1038/s41467-018-07641-9
40. Joshi T, Xu D (2007) Quantitative assessment of relationship between sequence similarity and function similarity. BMC Genomics 8:222. https://doi.org/10.1186/1471-2164-8-222
41. Kanehisa M, Sato Y (2020) KEGG Mapper for inferring cellular functions from protein sequences. Protein Sci 29:28–35. https://doi.org/10.1002/pro.3711
42. Krassowski M (2020) ComplexUpset [software]. Zenodo. https://doi.org/10.5281/zenodo.3700590
43. Le Strat Y, Tonon T, Leblanc C, Groisillier A (2023) Characterization of redox sensitive brown algal mannitol-1-phosphatases. Phycology 3:1–12. https://doi.org/10.3390/phycology3010001
44. Li Y, Gan S, Luo L et al (2023) Optimization of molasses and soybean meal content to enhance tetramethylpyrazine yield by *Bacillus* sp. TTMP20. Molecules 28:6515. https://doi.org/10.3390/molecules28186515
45. Lin Q, Pan F, Yang J et al (2026) Whole-genome sequencing and comparative genomics reveal antimicrobial potential and adaptive traits of *Bacillus velezensis* AM12. Funct Integr Genomics 26:27. https://doi.org/10.1007/s10142-025-01806-8
46. Ma Z, Hu J (2019) Complete genome sequence of a marine-sediment-derived bacterial strain *Bacillus velezensis* SH-B74, a cyclic lipopeptides producer and a biopesticide. 3 Biotech 9:162. https://doi.org/10.1007/s13205-019-1694-8

47. Madsen MA, Semerdzhiev S, Amtmann A, Tonon T (2018) Engineering mannitol biosynthesis in *Escherichia coli* and *Synechococcus* sp. PCC 7002 using a green algal fusion protein. ACS Synth Biol 7:2833–2840. https://doi.org/10.1021/acssynbio.8b00238
48. Mahdi I, Allaoui A, Fahsi N et al (2022) *Bacillus velezensis* QA2 potentially induced salt stress tolerance and enhanced phosphate uptake in quinoa plants. Microorganisms 10:1836. https://doi.org/10.3390/microorganisms10091836
49. Meier-Kolthoff JP, Göker M (2019) TYGS is an automated high-throughput platform for state-of-the-art genome-based taxonomy. Nat Commun 10:2182. https://doi.org/10.1038/s41467-019-10210-3
50. Meleshko D, Mohimani H, Tracanna V et al (2019) BiosyntheticSPAdes: reconstructing biosynthetic gene clusters from assembly graphs. Genome Res 29:1352–1362. https://doi.org/10.1101/gr.243477.118
51. Muras A, Larroze S, Mayer C et al (2021) Evaluation of the anti-fouling efficacy of *Bacillus licheniformis* extracts under environmental and natural conditions. Front Mar Sci 8:711108. https://doi.org/10.3389/fmars.2021.711108
52. Nguyen T, Kim T, Ta HM, Yeo WS, Choi J, Mizar P, Lee SS, Bae T, Chaurasia AK, Kim KK (2019) Targeting mannitol metabolism as an alternative antimicrobial strategy based on the structure-function study of mannitol-1-phosphate dehydrogenase in *Staphylococcus aureus*. mBio 10:e02660–e02618. https://doi.org/10.1128/mBio.02660-18
53. Petersen DS, Schultz M, Gorb SN, Heepe L (2020) A systematic investigation into the effect of fibrillar microstructures on the settlement and attachment strength of the bay barnacle *Balanus improvisus* under natural conditions. Appl Phys A 126:712. https://doi.org/10.1007/s00339-020-03870-2
54. Petrov K, Petrova P (2021) Current advances in microbial production of acetoin and 2,3-butanediol by *Bacillus* spp. Fermentation 7:307. https://doi.org/10.3390/fermentation7040307
55. Price MN, Wetmore KM, Waters RJ et al (2018) Mutant phenotypes for thousands of bacterial genes of unknown function. Nature 557:503–509. https://doi.org/10.1038/s41586-018-0124-0
56. Richter M, Rosselló-Móra R, Glöckner FO, Peplies J (2016) JSpeciesWS: a web server for prokaryotic species circumscription based on pairwise genome comparison. Bioinformatics 32:929–931. https://doi.org/10.1093/bioinformatics/btv681
57. Sánchez-Navarro R, Nuhamunada M, Mohite OS et al (2022) Long-read metagenome-assembled genomes improve identification of novel complete biosynthetic gene clusters in a complex microbial activated sludge ecosystem. mSystems 7:e00632–e00622. https://doi.org/10.1128/msystems.00632-22
58. Singh S, Subramanian S, Gupta N, Bajaj A, Manickam N (2024) Genomic insights on gene clusters and pathways for the biodegradation of plastic compounds: unravelling the metabolic versatility in a *Dietzia kunjamensis* IITR165. Curr Res Biotechnol 8:100258. https://doi.org/10.1016/j.crbiot.2024.100258

59. Stecker D, Hoffmann T, Link H et al (2022) L-proline synthesis mutants of *Bacillus subtilis* overcome osmotic sensitivity by genetically adapting L-arginine metabolism. Front Microbiol 13:908304. https://doi.org/10.3389/fmicb.2022.908304
60. Steinke K, Mohite OS, Weber T, Kovács ÁT (2021) Phylogenetic distribution of secondary metabolites in the *Bacillus subtilis* species complex. mSystems 6:e00057–e00021. https://doi.org/10.1128/msystems.00057-21
61. Terakawa A, Natsume A, Okada A et al (2016) *Bacillus subtilis* 5'-nucleotidases with various functions and substrate specificities. BMC Microbiol 16:249. https://doi.org/10.1186/s12866-016-0866-5
62. Tizabi D, Bachvaroff TR, Hill RT (2022) Comparative analysis of assembly algorithms to optimize biosynthetic gene cluster identification in novel marine actinomycete genomes. Front Mar Sci 9:914197. https://doi.org/10.3389/fmars.2022.914197
63. Tonkin-Hill G, MacAlasdair N, Ruis C et al (2020) Producing polished prokaryotic pangenomes with the Panaroo pipeline. Genome Biol 21:180. https://doi.org/10.1186/s13059-020-02090-4
64. Tonon T, Eveillard D, Prigent S et al (2017) Mannitol biosynthesis in algae: more widespread and diverse than previously thought. New Phytol 213:1573–1579. https://doi.org/10.1111/nph.14358
65. Tran DM, Huynh TU, Nguyen TH et al (2022) Molecular analysis of genes involved in chitin degradation from the chitinolytic bacterium *Bacillus velezensis*. Antonie Van Leeuwenhoek 115:215–231. https://doi.org/10.1007/s10482-021-01697-2
66. Vairagkar U, Nipanikar-Gokhale P, Mirza Y (2021) Genomic insights into biocontrol potential of edible seaweed-associated *Bacillus velezensis* MTCC 10456 from Gulf of Mannar. Arch Microbiol 203:2941–2952. https://doi.org/10.1007/s00203-021-02244-3
67. Wang T, Shi Y, Zheng M, Zheng J (2024) Comparative genomics unveils functional diversity, pangenome openness, and underlying biological drivers among *Bacillus subtilis* group. Microorganisms 12:986. https://doi.org/10.3390/microorganisms12050986
68. Wismayanti G, Sedjati S, Trianto A (2019) Aktivitas antagonis bakteri yang berasosiasi dengan teritip (*Balanus* sp.) terhadap bakteri *Escherichia coli* dan *Bacillus cereus* [Antagonistic activity of barnacle (*Balanus* sp.)-associated bacteria against *Escherichia coli* and *Bacillus cereus*]. J Kelaut Trop 22:49. https://doi.org/10.14710/jkt.v22i1.3244(in Indonesian)
69. Xiao F, Zhang Y, Zhang L et al (2024) Systematic review on marine carbon source-mannitol: applications in synthetic biology. Microbiol Res 289:127881. https://doi.org/10.1016/j.micres.2024.127881
70. Xu P, Xie S, Liu W et al (2020) Comparative genomics analysis provides new strategies for bacteriostatic ability of *Bacillus velezensis* HAB-2. Front Microbiol 11:594079. https://doi.org/10.3389/fmicb.2020.594079
71. Yi S-H, Hong S-P (2021) Characteristics of bacterial strains with desirable flavor compounds from Korean traditional fermented soybean paste (doenjang). Molecules 26:5067. https://doi.org/10.3390/molecules26165067

72. Zakataeva NP, Romanenkov DV, Yusupova YR et al (2016) Identification, heterologous expression, and functional characterization of *Bacillus subtilis* YutF, a HAD superfamily 5'-nucleotidase with broad substrate specificity. PLoS ONE 11:e0167580. https://doi.org/10.1371/journal.pone.0167580
73. Zeng Q, Zhao Y, Zhuang L et al (2025) Comparative genomics of *Bacillus velezensis* and *Bacillus subtilis* reveals distinction and evolution of lipopeptide antimicrobial gene clusters. BMC Genomics 26:1071. https://doi.org/10.1186/s12864-025-12234-0
74. Zhang M, Gu L, Cheng C et al (2018) Recent advances in microbial production of mannitol: utilization of low-cost substrates, strain development and regulation strategies. World J Microbiol Biotechnol 34:41. https://doi.org/10.1007/s11274-018-2425-8
75. Zheng J, Ge Q, Yan Y, Zhang X, Huang L, Yin Y (2023) dbCAN3: automated carbohydrate-active enzyme and substrate annotation. Nucleic Acids Res 51:W115–W121. https://doi.org/10.1093/nar/gkad328
76. Zhu N, Xia W, Wang G et al (2023) Engineering *Corynebacterium glutamicum* for de novo production of 2-phenylethanol from lignocellulosic biomass hydrolysate. Biotechnol Biofuels Bioprod 16:75. https://doi.org/10.1186/s13068-023-02327-x

Figures

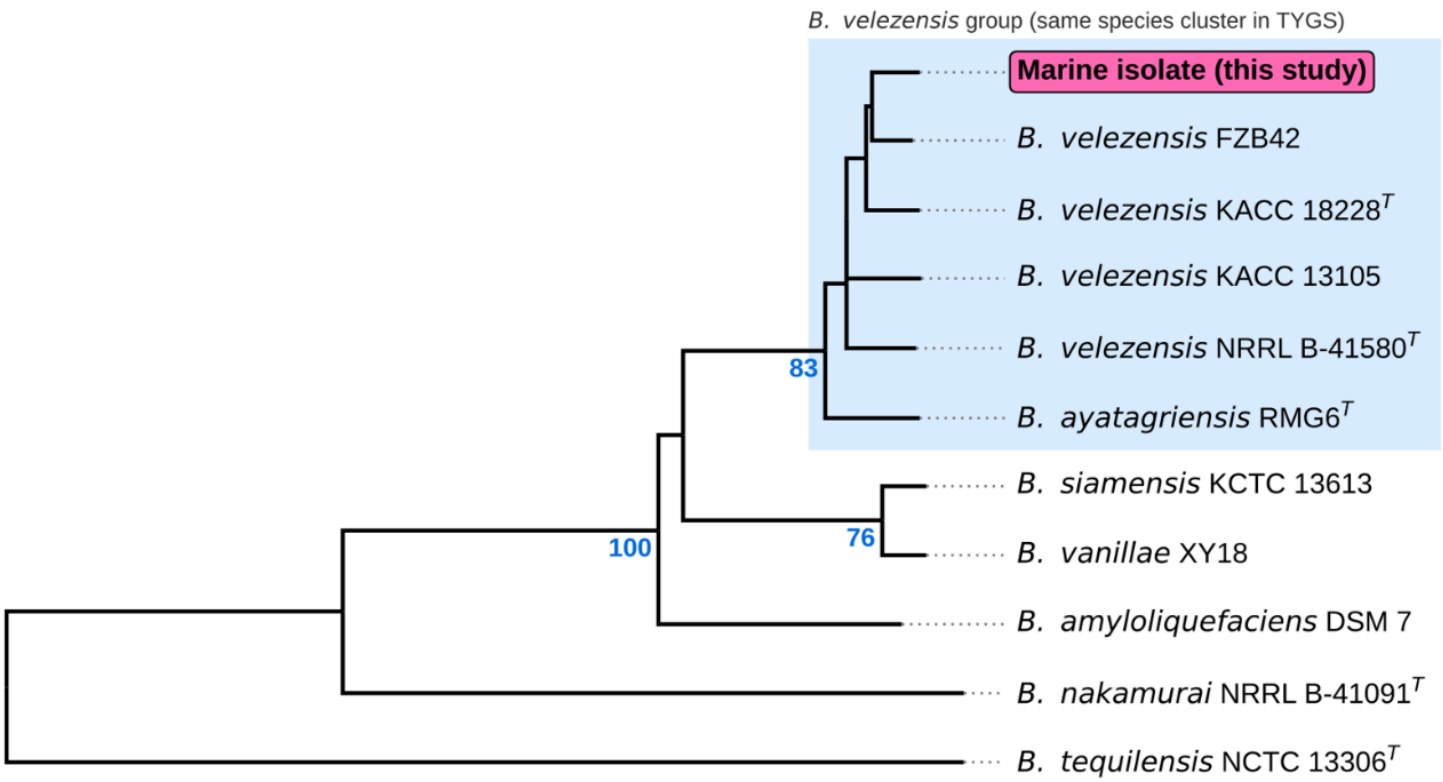

Figure 1

Genome-scale phylogenetic placement of the marine isolate

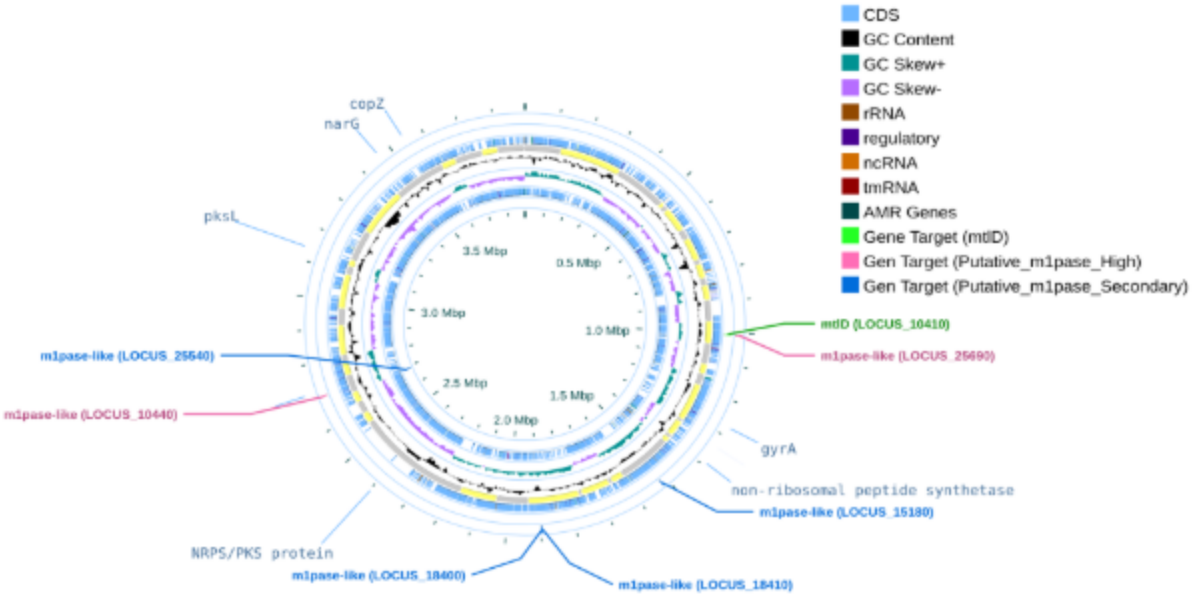

Figure 2

Circular representation of the draft genome of the barnacle biofilm-derived *Bacillus velezensis* isolate

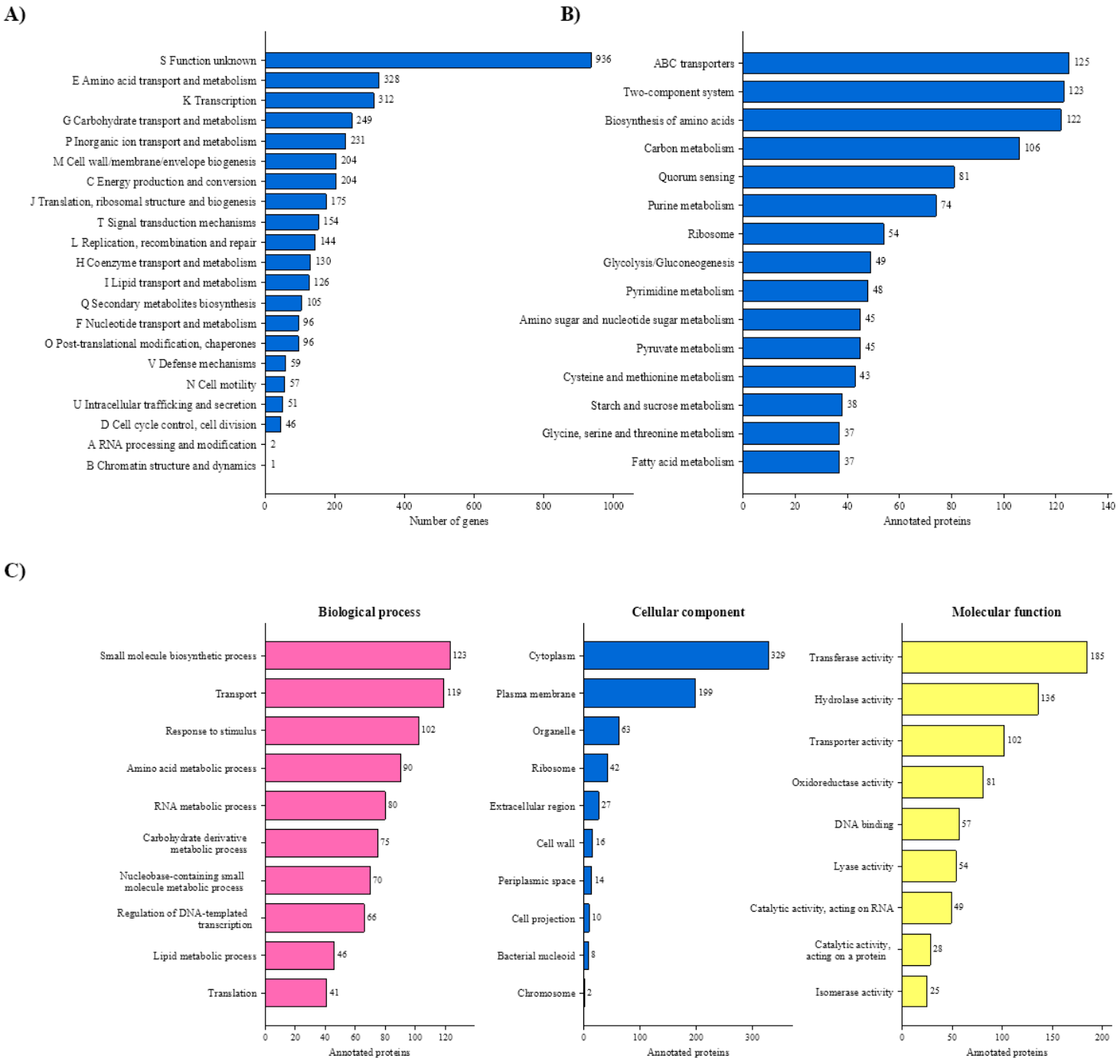

Figure 3

Functional annotation of the barnacle biofilm-derived *B. velezensis* isolate based on eggNOG-mapper. (A) COG functional categories; (B) top 15 KEGG pathways; (C) top GO terms in the biological process, cellular component, and molecular function categories.

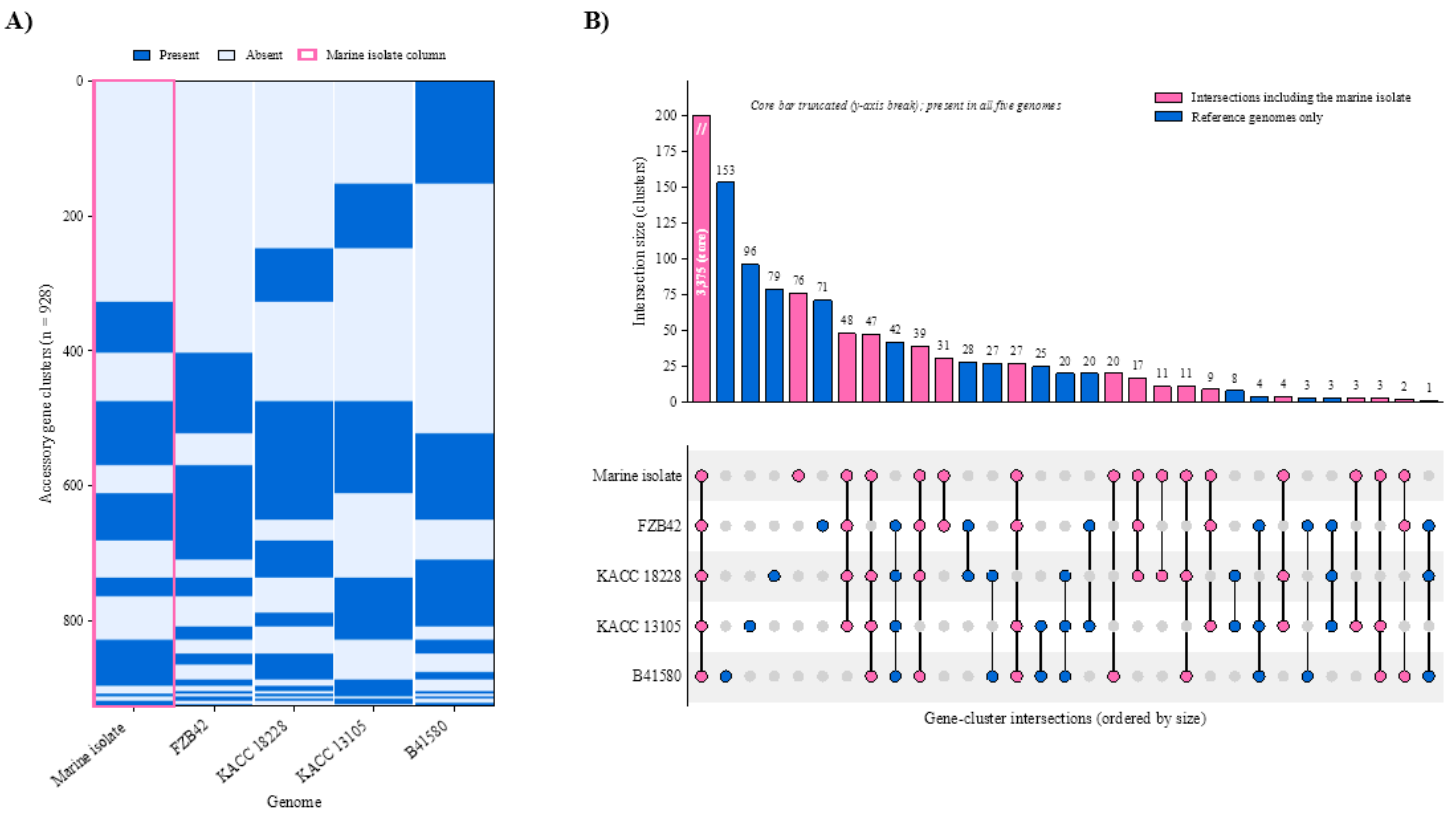

Figure 4

pan-genome analysis. (A) accessory gene presence–absence heatmap. (B) upset plot of gene cluster intersections among five genomes

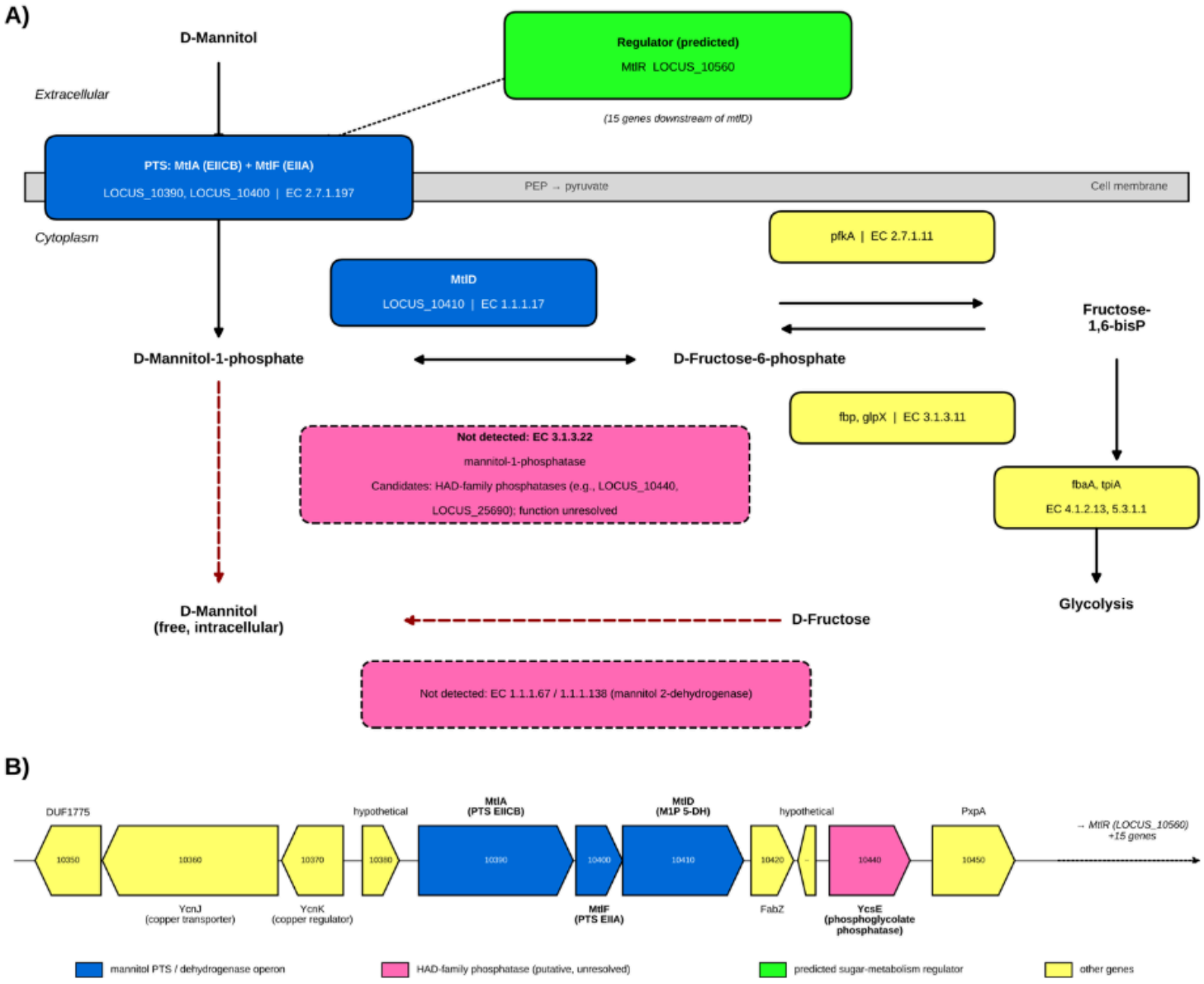

Figure 5

Genomic reconstruction in the marine isolate. (A) mannitol metabolic module and its genomic context. (B) gene neighbourhood

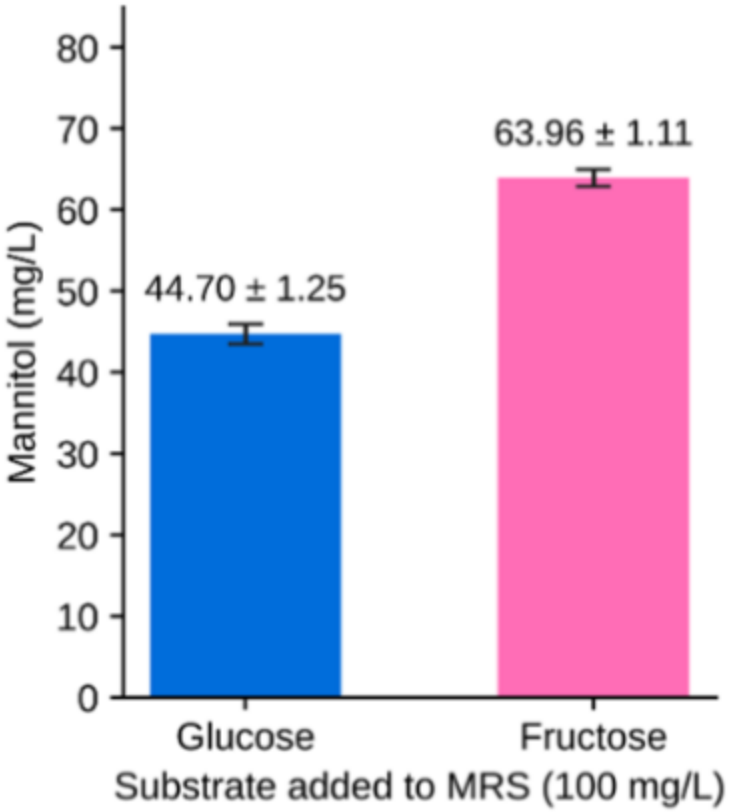

Figure 6

HPLC quantification of mannitol in cultures of the isolate

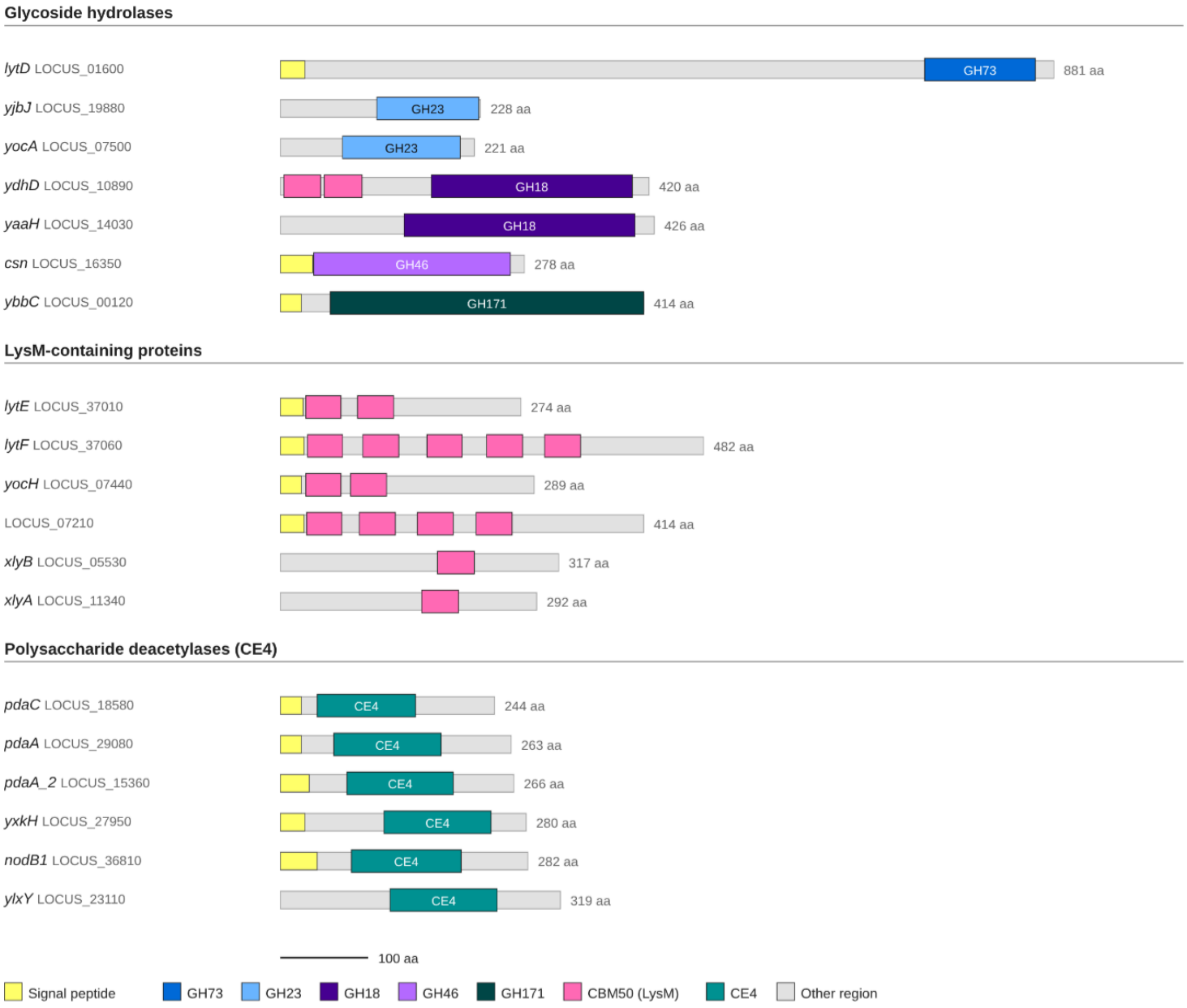

Figure 7

Domain organization of selected cell wall–active proteins in the marine isolate

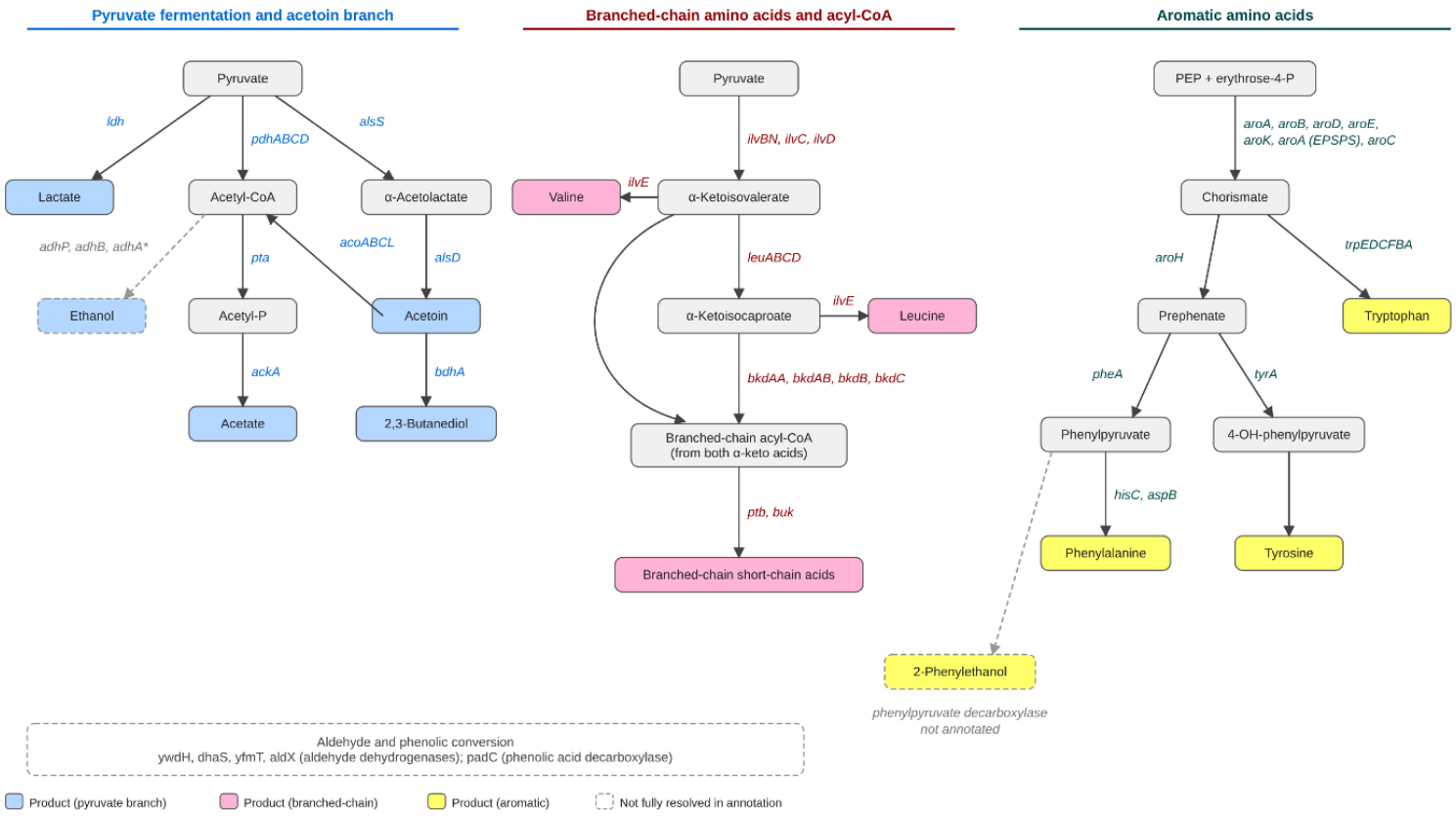

Figure 8

Fermentative and aroma-precursor pathways annotated in the marine isolate

Supplementary Files

This is a list of supplementary files associated with this preprint. Click to download.

- Supplementarymaterial.xlsx